# Remote free-carrier screening to boost the mobility of Fröhlich-limited 2D semiconductors

Thibault Sohier,[1] Marco Gibertini,[2] and Matthieu Verstraete[1]

[1] *nanomat/QMAT/CESAM and European Theoretical Spectroscopy Facility Universite de Liege, Allee du 6 Aout 19 (B5a), 4000 Liege, Belgium*

[2] *Dipartimento di Fisica Informatica e Matematica, Università di Modena e Reggio Emilia, Via Campi 213/a, I-41125 Modena, Italy*

(Dated: November 10, 2020)

Van der Waals heterostructures provide a versatile tool to not only protect or control, but also enhance the properties of a 2D material. We use ab initio calculations and semi-analytical models to find strategies which boost the mobility of a current-carrying 2D semiconductor within an heterostructure. Free-carrier screening from a metallic "screener" layer remotely suppresses electron-phonon interactions in the current-carrying layer. This concept is most effective in 2D semiconductors whose scattering is dominated by *screenable* electron-phonon interactions, and in particular the Fröhlich coupling to polar-optical phonons. Such materials are common and characterised by overall low mobilities in the small doping limit, and much higher ones when the 2D material is doped enough for electron-phonon interactions to be screened by its own free-carriers. We use GaSe as a prototype and place it in a heterostructure with doped graphene as the "screener" layer and BN as a separator. We develop an approach to determine the electrostatic response of any heterostructure by combining the responses of the individual layers computed within density-functional perturbation theory. Remote screening from graphene can suppress the long-wavelength Fröhlich interaction, leading to an almost constant mobility around 500 to 600 $cm^2/Vs$ for carrier densities in GaSe from $10^{11}$ to $10^{13}$ $cm^{-2}$. Notably, the low-doping mobility is enhanced by a factor 3. This remote free-carrier screening is more efficient than more conventional manipulation of the dielectric environment, and it is most efficient when the separator (BN) is thin.

## I. INTRODUCTION

Van der Waals heterostructures (VdWh) are becoming a device design paradigm in 2D materials applications[1,2]. The operating layer, performing the primary functionality, is included in a stack of other 2D layers fulfilling secondary roles like protection, gating or control. Encapsulating 2D materials in boron nitride (BN), for example, has already proven to be highly beneficial to the quality and cleanliness of the operating material's response[3,4]. The exciting prospect of including supporting 2D layers, to engineer the properties of the operating material beyond its intrinsic limits, has been much discussed in the past decade[5,6] but is only starting to be realized[7–10]. With this aim, one must understand, control, and exploit the interactions between all the layers within a VdWh. The present work takes a critical step towards this challenging task, in taking fully and quantitatively into account the mutual dielectric feedback between 2D layers.

VdWh engineering brings particularly interesting opportunities to electronic transport. High-mobility semiconductors are useful in many devices, especially when coupled with electrostatic doping[11–13], which allows to exploit a wide range of carrier densities, in a non-destructive and versatile way. In this context, depending on the application and the situation, the operating layer needs to perform well in many different doping regimes (hereafter, the nature of the doping should be understood as electrostatic). As discussed in the literature[14,15], it is a strong challenge for materials to display consistently good mobilities over a large range of carrier densities. This is particularly true for 2D materials whose scattering is dominated by the Fröhlich interaction with polar-optical phonons. This work explores the possibility of exploiting their integration in a VdWh to provide uniform performance over a range of doping levels.

Ab initio simulation of transport properties has shown promise in its ability to guide materials design. However, performing such studies for materials within a VdWh and over a large range of carrier densities remains a challenge. VdWh are difficult to simulate ab initio due to their multiple periodicities, entailing simulation supercells which are prohibitively large. The simulation of doping is also not obvious: Most ab initio electron-phonon scattering calculations in semiconductors are done in the zero doping limit. The ability to self-consistently simulate electron-phonon interactions in electrostatically doped 2D materials was recently developed[16], but remains computationally affordable only when Fermi surfaces are large enough, i.e. at large enough doping. Models to bridge the gap between the zero and large doping regimes are still lacking.

Here we propose a step towards ab initio simulation of transport in VdWh devices over a large range of doping. In particular, we propose a framework to deal with "screenable" contributions to electron scattering by phonons, as those are likely to be most affected by VdWh integration and doping. We further focus on one of the most common and important type of screenable electron-phonon coupling: the Fröhlich interactions with polar-optical phonons. A semi-analytical scheme is used to treat the electrostatics of the VdWh including dielectric

and free-carrier screening from different layers. The response of each individual layer to a generic potential perturbation is computed in Density Functional (Perturbation) Theory (DFT / DFPT), then they are combined in a model for the full response of the VdWh to the Fröhlich potential(s). Dielectric models of VdWh have been developed in the past[17–19], with a focus on quantities like the dielectric function. We propose another formal framework, with a focus on the potentials generated by electron-phonon interactions, and apply it to a new problem: phonon-limited electronic transport.

This VdWh electrostatics model is used to demonstrate a solution to the aforementioned materials design challenge, i.e. high mobility over a wide range of doping regimes, using the prototypical example of GaSe. In a recent work[15], the outstanding transport performance of GaSe was predicted in the high doping regime. Transport in this material is limited by the Fröhlich interaction, and the high mobility at high doping relies largely on the screening of this interaction by free-carriers added to GaSe. This is confirmed in the present work by showing a decrease of intrinsic mobility by more than a factor 3 in the low doping regimes. It is then shown that this decrease can be avoided by putting GaSe in proximity with a metal, providing free-carrier screening externally, irrespective of GaSe's doping. In particular, we propose a GaSe/BN/graphene heterostructure, with doped graphene as a "screener" layer and BN as a separator. The principle of proximity free-carrier screening has recently been used to tune the band gap of semiconductors[20] and to manipulate electron-electron interaction in graphene[10]. We use it here to engineer electron-phonon interactions within the current-carrying 2D semiconductor.

This paper is structured as follows. In section II, we use the case of GaSe to discuss the doping-dependent performance of 2D layers in which the Fröhlich interaction dominates electron-phonon scattering, and demonstrate that the lack of intrinsic free-carrier screening at low doping leads to very low mobility. In section III, we develop the electrostatic model that allows us to calculate the response of the full VdWh from the ab initio response of each layer computed independently. Finally, in section IV we apply this approach to the GaSe/BN/Graphene heterostructure and show that the mobility can be kept virtually constant at a high value between 500 and 600 $cm^2/Vs$, at carrier densities from $10^{11}$ to $10^{13}$ $cm^{-2}$.

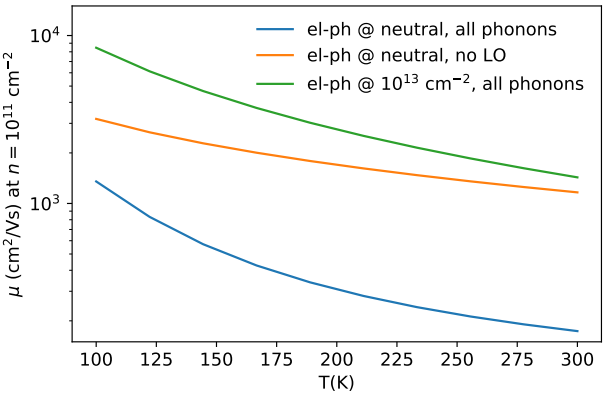


FIG. 1. Ab initio mobility versus temperature in neutral GaSe, in the $n \to 0$ limit (reached at $n \simeq 10^{11}$). The mobility without the longitudinal optical (LO) phonons is plotted to show that scattering with this mode limits transport. Finally, we also compute mobility in a fictitious system by using the EPIs of GaSe doped at $n = 10^{13}$ $cm^{-2}$ while simulating the transport at $n = 10^{11}$ $cm^{-2}$. This shows that free carrier screening of the EPIs, induced by doping the layer itself, is able to suppress the main electron-phonon scattering mechanisms and increase the mobility.

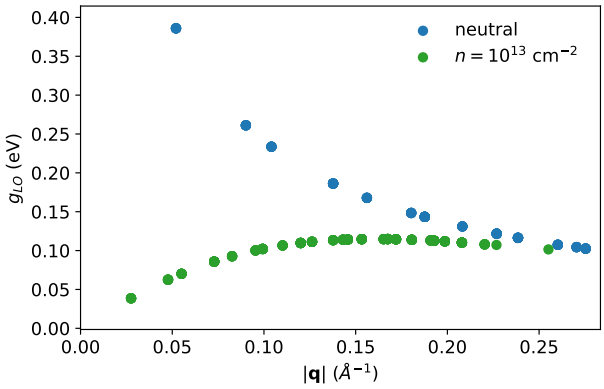


FIG. 2. EPIs between the LO mode and states at the bottom of GaSe's conduction band, computed within DFPT for neutral and doped GaSe, as a function of the phonon momentum. Other modes have non-negligible coupling (LA and $A_{1g}$), but LO clearly dominates scattering through the Fröhlich interaction. It is strongly affected by free-carrier screening: in the doped case, the coupling vanishes as $\Gamma$ and overall it barely reaches a 10% of the maximum value in the neutral case ($\sim 1.124$ eV at $\Gamma$).

## II. FRÖHLICH LIMITED 2D SEMICONDUCTORS

The broad class of materials concerned by this work are 2D semiconductors for which the electronic transport performance is limited by scattering mechanisms which are sensitive to free-carrier screening. It is not obvious to further qualify this class as a whole, which hosts a variety of different members. Focusing on intrinsic scattering mechanisms driven by electron-phonon interactions (EPIs), multi-valley materials can usually be excluded, since inter-valley EPIs are often strong[21,22], and at momenta larger than the size of the Fermi pocket that characterizes the free carriers providing the screening. In this large momentum regime, free-carrier screening is inefficient even if the EPI are sensitive to it. In single valley materials (up to quite high chemical potentials), it is

reasonable to assume that free-carrier screening will be efficient on screenable EPIs. These include the Fröhlich, piezoelectric, and acoustic "deformation-potential" EPIs. Others, like those responsible for graphene's intrinsic transport properties, are altogether insensitive to screening. Which kind of EPI dominates transport will depend on the specific material. This work focuses on 2D materials in which the dominant EPI is the Fröhlich interaction between electrons and polar-optical phonons, usually the longitudinal optical (LO) modes. Fröhlich EPIs concerns any semiconductor in which the atoms of the unit-cell carry different Born effective charges (BECs). This includes any non-elemental material, but also elemental materials with some factor disrupting the balance between the atoms[23]. Fröhich EPIs increase as: BECs increases, screening decreases, or the LO phonon energy decreases. Since they are mediated by long-range electric fields, they are screenable. It is certainly one of the most pervasive and critical source of EPI[24,25], and it has been extensively modelled in both 3D[26–30] and 2D[31], with parameters for the BECs and the dielectric properties. In 3D bulk materials, the Fröhlich EPI diverges as the inverse of the phonon momentum in the long wavelength limit[32], which can have a strong impact on scattering. While the EPI stays finite in 2D systems, it still undergoes a sharp increase at small momenta, and the Fröhlich EPI can easily dominate all other mechanisms as in 3D.

In the 2D framework, the long wavelength Fröhlich electron-phonon coupling (see App. A 3) can be thought of as the ratio of a parameter depending on BECs and mildly on momentum, and the dielectric function $\epsilon(q)$, which accounts for both the environment and the material containing the electrons involved. The dielectric function in the long wavelength limit ($q \to 0$) can be modeled as $1 + \alpha q$ for a 2D material in vacuum, but the present work relies on a more detailed and realistic model. One general behavior is that, in 2D, the dielectric function is dominated by the response of the environment for $q \to 0$ and by that of the 2D material for $q \to \infty$.

In a recent work[15], eleven of the best conductors within a database of exfoliable materials[33–35] were identified. Seven of them display rather large BECs and strong Fröhlich EPIs. Since the calculations were done at a relatively large doping, these EPIs were screened by local free carriers, and did not affect drastically the conductivity. However, those same materials can be expected to have much lower mobilities at low doping, when screening is ineffective.

A prototypical example is GaSe (see Ref. 33 for basic properties). For reference, the room temperature mobility at $n = 10^{13}$ cm$^{-2}$ was computed to be $\mu \simeq 600$ cm$^2$/Vs[15], placing it among the very best performing 2D semiconductors at high doping. We now look at electronic transport in GaSe in the zero doping limit. EPIs are computed in DFPT and the full energy- and momentum-dependent Boltzmann transport equation is solved iteratively as described in Ref. 21. To compute the zero doping limit, we use $n = 10^{11}$ cm$^{-2}$, as we found that the mobility is stable within 2% below that value. The mobility as a function of temperature is shown in Fig. 1 for 3 different sets of EPIs (2 of them fictitious). In the first (realistic) system, we use the EPI matrix elements as computed in the neutral material ($n = 0$). This represents the standard small doping limit. The room-temperature mobility is $\mu \simeq 174$ cm$^2$/Vs, much lower than the high doping value. For the second (fictitious) system we use the same EPI, but without the Fröhlich-inducing phonon LO. The mobility increases by an order of magnitude, clearly showing that Fröhlich is limiting the mobility. In the third system, we use the EPI computed in GaSe at a doping of $n = 10^{13}$ cm$^{-2}$ in Refs. 15 and 36. This system is fictitious because the BTE is solved with a doping level ($n = 10^{11}$ cm$^{-2}$) different from the one used in EPI calculations ($n = 10^{13}$ cm$^{-2}$). It is instructive since it shows that, keeping all other factors the same, using the EPIs from the doped system leads to an order of magnitude increase in the mobility. This is due to the screening of the Fröhlich EPI by the high density of added free carriers, as confirmed in Fig. 2 showing the coupling of the LO mode $g_{LO}(|\mathbf{q}|)$ for the neutral and doped systems. It can thus be inferred that free-carrier screening of the Fröhlich EPI would enhance the mobility of GaSe in the low doping limit. Since there are not enough intrinsic free carriers in GaSe in the low doping regime, one would need an external source of free-carrier screening. We propose to place GaSe in a VdWh with doped graphene to screen the Fröhlich EPIs remotely. To demonstrate this, we first develop a model for the complete electrostatics of such systems.

## III. VAN DER WAALS ELECTROSTATICS MODEL

This section describes a semi-analytical model parametrized with density-functional perturbation theory (DFPT) to solve the electrostatics (i.e. the response to a static electric field perturbation) of a VdWh in the presence of both dielectric and free-carrier screenings. We are especially interested in the response to the Fröhlich potential generated by polar optical phonons. The entire VdWh would be prohibitively expensive to simulate in DFPT, especially with the very fine wave vector grids needed for transport. This model aims at re-constructing the full response of a VdWh from the response of each individual layer, which can be reasonably computed in DFPT. The process relies on a response function model, which is isotropic and $q$ dependent in the plane and has a flexible profile in the out-of-plane direction. Ultimately, we are interested in the screened potential felt by electrons in the operating layer, which will dictate its transport properties and the device performance. More formal details can be found in App. A.

Although any combination of 2D layers can be studied, we focus here on GaSe/BN/Graphene systems, as represented in Fig. 3. Monolayer GaSe (gap $\approx 1.8$ eV within

the GGA-PBE approximation to the DFT exchange-correlation functional) is the operating material in which electronic transport occurs. Carrier densities ranging from the $n \to 0$ limit up to $n = 10^{13}$ cm$^{-2}$ are considered in the GaSe layer. Doped monolayer graphene is the "remote screener", with a fixed carrier density of $n = 5\ 10^{13}$ cm$^{-2}$, which will be referred to later on via the notation Gr(doped). BN has a large gap of $\approx 4.7$ eV in GGA-PBE and is routinely used in 2D VdWh as an encapsulator or gate dielectric. It is necessary here to electrically isolate the operating material from the remote screener and avoid charge transfers. Both monolayer and multilayer BN are studied in the following.

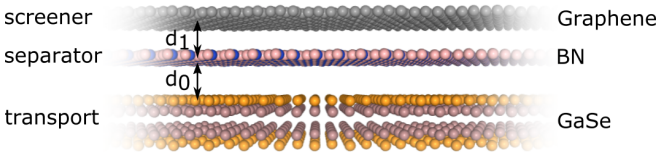


FIG. 3. Schematic view of the system studied. The transport layer (here GaSe or more precisely $Ga_2Se_2$, which is composed of too sublayers) is the operating 2D material that carries the current. The screener layer (doped graphene) provides free-carrier screening remotely. Finally, the separator (BN) electrically insulates the operating material and the screener. The interlayer distances $d_0$ and $d_1$ can be different in general, but they are both fixed to $d = 3.4$ Å in this work. Although monolayer BN is represented, multilayer BN is also considered.

The electrostatics of the system are determined from the response of each individual layer to electric fields perturbations. Given the in-plane periodicity and symmetry of the system, the corresponding perturbing potential is periodic in the plane, and written $V(q, z)$ where $q$ is the norm of the in-plane momentum, and $z$ the out-of-plane real-space variable. Doped graphene responds like a metal, with perfect screening of in-plane electric fields in the long wavelength limit. BN also brings a $q$-dependent dielectric response (inefficient at small $q$, and similar to bulk BN at large $q$). The operating layer, GaSe, responds like a dielectric at low doping, and a metal at high doping. The dielectric response of neutral GaSe is computed directly in DFPT, and the contribution of potential free-carriers (as induced in GaSe by electrostatic doping) is added on top. As detailed in App. A, The central quantity characterizing each layer's behavior is the interacting response function, assumed to be of the form:

$$\begin{aligned}\chi(q, z, z') =& Q(q) f(q, z - z_0) f(q, z' - z_0) \\ &+ P(q) g(q, z - z_0) g(q, z' - z_0)\end{aligned} \quad (1)$$

$Q, f$ characterize the monopole contribution to the response, while $P, g$ represent the dipole part. $f$ is an even function of $z$, and describes the normalized spatial profile of the material's response to a constant potential $V(q, z) \propto 1$. $Q$ is the associated $q$-dependent amplitude of this response. Similarly, $g$ is odd and, along with the amplitude $P$, they represent the response to a linear potential $V(q, z) \propto z$ ($q$-dependent vertical electric field). Those functions are computed for each individual layer in DFPT for the range of momenta $q$ that eventually enter the Boltzmann transport equation. Isotropy is assumed, so only one arbitrary direction is used for the momentum.

The responses of each layer are then combined in an electrostatic model of the VdWh, as detailed in section A 2. This is done by making an "interlayer mean-field" approximation. In practice, we assume that each layer responds to an effective external potential made of the global external potential plus the sum of the induced potential from all other layers. This assumption allows us to define a simple system of equations that we then solve numerically, see App. A 2.

Since they have finite Born effective charges, both BN and GaSe will generate Fröhlich EPIs. Electrons in GaSe thus couple to polar-optical phonons in both GaSe and BN, the latter being remote. Phonons are not explicitly simulated in the VdWh electrostatics model. They are assumed to be unchanged from the isolated layers to the VdWh (no interlayer hybridization of modes). The potential they generate is recreated from DFPT calculations, and used to perturb the VdW electrostatics model. One improvement over previous models[31] is to exploit the parametrization of the layers' dielectric response to model the profile of the polarization density that generates the Fröhlich EPI, as detailed in App. A 3. Only first order dipole potentials are considered, quadrupole contributions[37–40] are neglected. In principle, multilayer materials generate several polar-optical phonons with different phase shifts in the layers[41]. Here we focus on the mode with largest Fröhlich EPI, in which all layers are in phase. We make the adiabatic approximation, allowing us to treat phonons as a static perturbation ($\omega = 0$).

The Fröhlich potential and the responses are assumed to be isotropic in the range of $\mathbf{q}$ vectors considered. This is valid for all layers here, as is well-known for graphene and BN[31,41,42], and also in GaSe as we can see in Fig. 2. Indeed, the $\mathbf{q}$ vectors calculated within DFPT sample the whole Brillouin zone, along all possible directions; the fact that the scatter plot gives a line demonstrates isotropy.

Interlayer distances are chosen to be 3.4 Å, understood as the geometric distance between the outermost atomic planes of successive 2D materials. For BN and graphene, there is only one atomic plane. For GaSe, there are 4, the outermost being 2.4 Å away from the center of the layer.

For clarity, we compare our formalism with the existing Quantum Electrostatic Heterostructure (QEH) model[17,19] in App. A 5. They both achieve a similar general purpose: to compute the dielectric response of a Van der Waals heterostructure from the ab initio response of each individual layers. However, the approaches differ on several levels, mostly related to our focus on $z$-dependent

potentials rather than averaged quantities like the dielectric constant. In addition, we apply this approach to a different perturbation here, namely the Fröhlich EPI.

Ab initio calculations of structures, ground states and dielectric responses are performed with Quantum ESPRESSO[43,44] (QE). Full electron-phonon interactions and transport calculations in neutral and doped GaSe were done for comparison, with ultrasoft pseudopotentials from the SSSP library[45] (efficiency version 0.7). The Phonon code of QE has been modified to compute the dielectric response of each layer. More specifically, the phonon perturbation is replaced by the potentials in Eq. (A3) of App. A 1. Those modifications are similar to a previous work[42], with the addition of the dipole perturbation. Dielectric responses were computed using optimized norm-conserving Vanderbilt pseudopotentials[46] from the pseudo-Dojo library[47], as the modifications of the Phonon code have not been implemented yet for other types of pseudopotentials. We use the AiiDA materials informatics infrastructure[48,49] to manage calculations and store data. The solution of the VdWh electrostatics model is implemented in Python.

## IV. RESULTS

Our approach provides a clear and intuitive physical understanding of the VdWh in terms of electrostatics. Fig. 4 illustrates this by showing the potentials solving the model in the most relevant configuration: GaSe(neutral)/BN/Gr(doped) perturbed by a Fröhlich potential from GaSe's polar-optical phonons. We select two momenta at the extrema of the interval considered in this work. At small $q$, graphene's response is prominent. Indeed, the perturbation extends far in the out-of-plane direction and graphene is metallic, so the induced potential is (negatively) large. We also note that since the bare Fröhlich potential varies over the dielectric thickness of the graphene layer, graphene's response is not symmetric with respect to the middle of the layer. Responses from BN and GaSe both display clear dipole-like features with positive and negative electric field regions. For GaSe, the dipole component originates mostly from the response to graphene's induced potential, which varies significantly over GaSe's thickness, yielding a finite electric field. Despite the dipolar feature, GaSe's response clearly does not average to zero, indicating that there is a significant monopole component to its response as well, this time triggered mostly by the bare Fröhlich perturbation. BN's response also includes both monopole and dipole components, but is closer to a purely dipolar one. BN feels two main potentials with finite derivatives: the bare Fröhlich from GaSe and the induced response from graphene. They have counteracting effects, and the sign of the dipolar response confirms that the bare Fröhlich from GaSe dominates.

At large $q$, GaSe itself performs most of the screening, with a small contribution from BN on one side. The induced potential from graphene is very weak compared to the smaller $q$ case, due to the fact that the bare Fröhlich potential decays more rapidly (as $e^{-q|z-z_{\mathrm{GaSe}}|}$) in the out-of-plane direction and doesn't reach graphene. The screened Fröhlich potential is slightly smaller (more screened) on the side of GaSe adjacent to BN. This was true for the small $q$ case as well, and is a general and intuitive feature: the screening is more efficient towards the separator and screener layers. However, the difference is within 2%: despite the asymmetry of the induced potentials (with respect to their respective layers), the total screened potential ends up quite flat within each layer. This indicates that the dipole response of each layer is near-perfect, meaning that any perpendicular electric field is almost fully compensated.

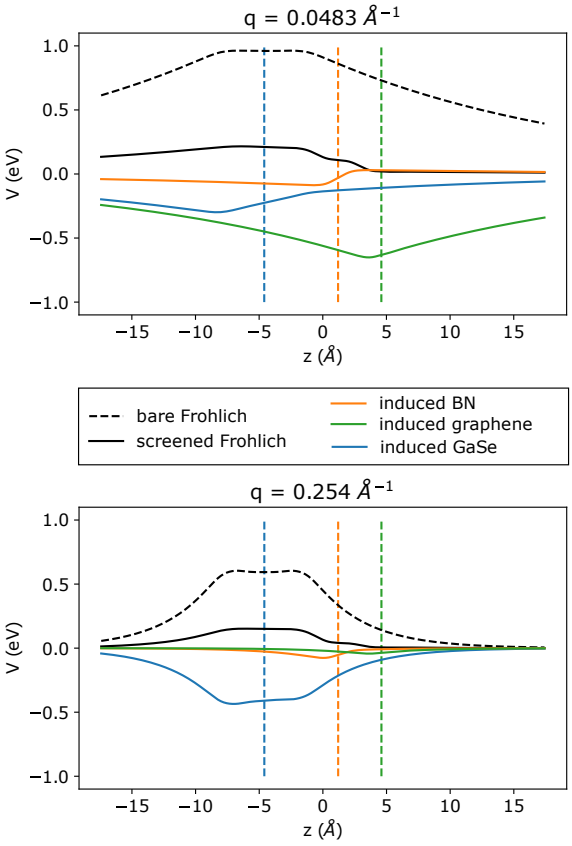


FIG. 4. Bare, induced and screened potentials for the most relevant configuration: GaSe(neutral)/BN/Gr(doped), in response to the Fröhlich potential generated by GaSe, at two values of momentum. The induced potential is separated into contributions from each layer, with their position indicated by the vertical dashed lines. Note that strictly speaking, $V$ is the potential energy of a test charge $e$ in eV, rather than an electric potential.

In Fig. 5, the electrostatics are solved in different systems, gradually adding the key layers and observing the effects on the screened Fröhlich EPIs as felt by

GaSe's electrons. Those are computed by averaging the full screened potential over the GaSe layer, as detailed in App. A 3. First, in neutral GaSe alone, the Fröhlich potential is only screened dielectrically by GaSe. Second, in GaSe(neutral)/BN, there is a relatively weak additional dielectric screening from BN: this represents the standard type of screening one can expect from a dielectric environment (substrate or encapsulator). An additional remote Fröhlich potential from BN comes into play. Although it is quite strong, its consequence on transport is limited by the fact that the energy of the associated phonon is very large ($\sim 0.19$ eV). Indeed, injecting this coupling into a simple Fermi golden rule, the scattering rate of a state at the Fermi level is proportional to $n_{\rm BE}(\hbar\omega) \times (1 - n_{\rm FD}(\varepsilon_F + \hbar\omega)) + (n_{\rm BE}(\hbar\omega) + 1) \times (1 - n_{\rm FD}(\varepsilon_F - \hbar\omega))$ where $n_{\rm BE}$ and $n_{\rm FD}$ are the Bose-Einstein and Fermi-Dirac occupation functions for phonons and electrons, respectively. Up to high temperature, there will be few phonons to absorb ($n_{\rm BE}(\hbar\omega) \ll 1$), and phonon emission (second term) will be limited by the fact that states at $\varepsilon_F - \hbar\omega$ are mostly occupied ($1 - n_{\rm FD}(\varepsilon_F - \hbar\omega) \ll 1$). In fact, based on LO frequencies in GaSe and BN (200 and 1500 cm$^{-1}$, respectively), this expression allows to estimate that for a equal EPI the scattering from BN's phonons will 3 orders of magnitude less efficient than GaSe's at room temperature. Third, in GaSe(neutral)/BN/Gr(doped), the doped graphene sheet acts as a remote " screener" layer. There is now some metallic screening, with the coupling vanishing as $q \to 0$. The efficiency of this remote screening is limited in $q$, as seen when comparing the induced potentials from graphene at small and large $q$ in Fig. 4. The efficiency is related to the inverse of the distance between graphene and GaSe. Still, the remote screening is most essential in the critical low doping limit of GaSe, when the Fermi surface and $\mathbf{q}$ vectors relevant for transport in GaSe are small. Thus, reducing the sharp increase at $q = 0$ is enough to suppress the electron-phonon scattering.

Fig. 6 shows the effect of the number $N$ of BN layers. As $N$ increases, so does the intensity of the remote Fröhlich EPIs, as contributions from each layer add up. The efficiency of remote screening from graphene is limited to momenta smaller than a certain critical $q$, which decreases with increasing distance $d$ between GaSe and graphene. This effect can be roughly estimated as follows. Both the bare Fröhlich potentials felt by graphene and the induced potential from graphene felt by GaSe decay as $e^{-qd}$. Remote screening becomes inefficient when $e^{-q\times(2d)} \ll 1$, that is when $q \gg \frac{1}{2d}$, where $d = (N + 1) \times 3.4$ Å in our model. Thus, from an electrostatics standpoint, it is better to minimize the number of layers. Of course, what is feasible and optimal in a practical device may depend on other parameters.

Fig. 7 shows the variation of the EPIs in GaSe($n$)/BN/Gr(doped) with respect to carrier density $n$

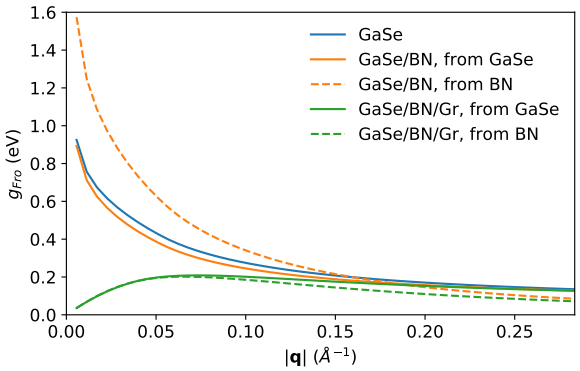


FIG. 5. Fröhlich EPIs from polar-optical phonons in both GaSe (plain) and BN (dashed), as felt by electrons in GaSe, in different setups: GaSe(neutral) alone, GaSe(neutral)/BN, and GaSe(neutral)/BN/Gr(doped), with at $n = 5\ 10^{13}$ cm$^{-2}$ in graphene. Fröhlich potentials coming from both GaSe and BN are considered, but always "as felt by GaSe electrons", that is, the Fröhlich potential is always averaged over the GaSe layer.

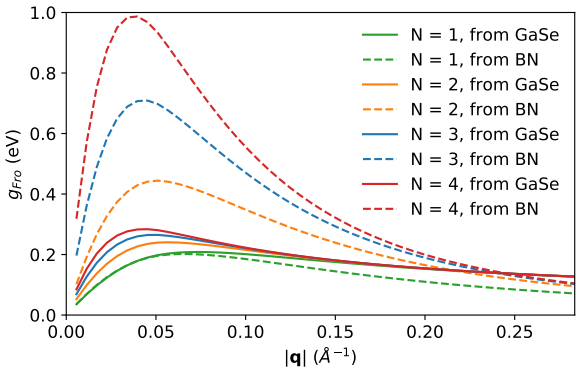


FIG. 6. Fröhlich EPI from polar-optical phonons in both GaSe (plain) and BN (dashed), as felt by electrons in GaSe, in GaSe(neutral)/BN/Gr(doped), changing the number of BN layers (N). Most of the screening comes from free carriers in graphene, and it becomes less efficient as N increases and the distance between graphene and GaSe increases. The increase in the Fröhlich EPI coming from polar-optical phonons in BN is more drastic because the bare Fröhlich potentials from each BN layer add up.

in GaSe. Screening from the free carriers added in GaSe is modeled as described in App. A 4 at room temperature. First, note that as $n$ increases, the Fermi surface gets larger, and the momenta most relevant to transport ($q \approx 2k_F$) increase. The efficiency of intrinsic free-carrier screening also follows the size of the Fermi surface and extends to larger $q$. As a result, the Fröhlich EPIs (intrinsic and remote) at momenta relevant for transport are always significantly screened.

In Fig. 8, we inject the modelled Fröhlich EPIs of the last system, GaSe($n$)/BN/Gr(doped), back into the

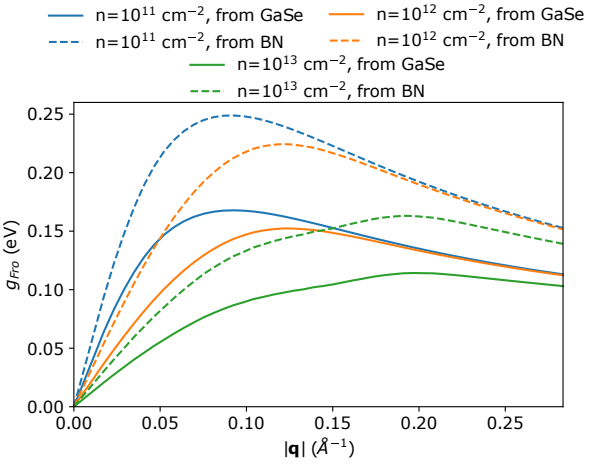


FIG. 7. Fröhlich EPI from polar-optical phonons in both GaSe (plain) and BN (dashed), as felt by electrons in GaSe, in GaSe($n$)/BN/Gr(doped), changing the doping in GaSe $n$. As the carrier density increases, free-carrier screening from electrons in GaSe comes into play, ensuring the ability of the system as a whole to screen EPIs at the larger momenta involved in transport.

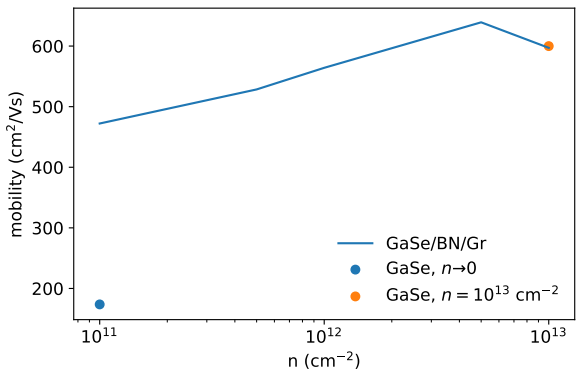


FIG. 8. Mobility versus electrostatic doping, replacing $g_{LO}$ by our model for the Fröhlich EPIs within the VdW heterostructure. Remote EPIs from BN are also added. The dots are direct, full DFPT calculations for a monolayer GaSe in the low doping limit (EPIs computed in neutral GaSe, transport solved at $n = 10^{11}$ cm$^{-2}$) and at high doping ($n = 10^{13}$ cm$^{-2}$).

Boltzmann transport solver and look at the mobility as a function of GaSe doping $n$. Note that the mobility predicted by our model at $n = 10^{13}$ cm$^{-2}$ is quite close to the one computed directly in DFPT in GaSe alone at the same doping. This indicates that: i) as expected, remote Fröhlich EPIs from BN stay negligible with respect to those from GaSe; ii) other potentially screened EPIs only play a minor role in determining the mobility at room temperature. In addition to preserving good performance at high doping, the benefits of the VdWh are obvious, since instead of degrading towards the neutral isolated limit at low doping, the mobility stays relatively constant. As carrier density decreases, the intrinsic free-carrier screening lost from depleting carriers in GaSe is compensated by remote free-carrier screening from graphene. Remote screening thus extends the outstanding performance of GaSe to the full range of doping typically achievable experimentally.

## V. CONCLUSION

We have developed a semi-analytical model to simulate the electrostatic response of any VdWh. The model is parametrized via the DFPT density-response of each individual layer to a monopole and dipole perturbation potential. We use this model to explore the possibility of using metallic 2D layers in VdWh (e.g. doped graphene) to induce free carrier screening remotely in a current carrying semiconducting layer. This is particularly relevant for 2D semiconductors with transport properties limited by screenable EPIs such as the Fröhlich interaction. In particular, such materials would typically showcase excellent transport performance in presence of free-carrier screening (e.g. at high-doping), but lower mobilities in its absence (low doping). Using GaSe as a prototypical example, we show that integrating it in a VdWh device with doped graphene as a remote screener and BN as a separator enhances the mobility at low doping. The mobility is thus maintained at a consistently high value of $\sim 500 - 600$ cm$^{-2}$/Vs on a wide range of carrier concentrations.

## ACKNOWLEDGMENTS

We are grateful to Matteo Calandra for his help with the initial implementation of the linear response to a monopole perturbation in the Quantum ESPRESSO code. We acknowledge that the results of this research have been achieved using the DECI resource ARCHER UK National Supercomputing Service with support from the PRACE aisbl. Simulation time was also awarded by PRACE (project id. 2020225411) on MareNostrum at Barcelona Supercomputing Center - Centro Nacional de Supercomputación (The Spanish National Supercomputing Center)". Computational resources have been provided by the Consortium des Equipements de Calcul Intensif (CECI), funded by the Fonds de la Recherche Scientifique de Belgique (F.R.S.-FNRS) under Grant No. 2.5020.11 and by the Walloon Region. T.S. acknowledges support from the University of Liege under Special Funds for Research, IPD-STEMA Programme. M.G. acknowledges support from the Italian Ministry for University and Research through the Levi-Montalcini program. M.J.V. gratefully acknowledges funding from the Belgian Fonds National de la Recherche Scientifique (FNRS) under PDR grant T.0103.19-ALPS.

## Appendix A: Model details

This appendix details technical aspects of the electrostatics model: the extraction and parametrization of each monolayer's response from DFPT; the semi-numerical scheme to combine those responses and solve the electrostatics of the VdWh; the model for the perturbing Fröhlich potential; the inclusion of doping-induced free-carrier screening. A quick comparison of this model with the existing QEH method[17,19] is also provided.

### 1. Monolayer response from DFPT

In-plane periodicity and symmetry suggests we Fourier transform quantities in-plane and keep the out-of-plane real-space variable: $(x, y, z) \to (\mathbf{q}, z)$. Since the systems are assumed isotropic in the plane, we further simplify and use $q = |\mathbf{q}|$. The response of the layer to a generic perturbing potential is written as:

$$\begin{aligned} V_{\text{ind}}(q,z) &= v_c(q) \int e^{-q|z-z'|} \delta n(q,z') dz' \\ \delta n(q,z) &= \int \chi(q,z,z') V_{\text{ext}}(q,z') dz' \end{aligned} \tag{A1}$$

where $v_c(q) = \frac{2\pi e^2}{q}$ is the Coulomb kernel in 2D and the (interacting) response function $\chi$ is written as in Eq. (1). The profile are normalized as follows:

$$\int f(q, z - z_0) dz = \int (z - z_k) g(q, z - z_k) dz = 1 \tag{A2}$$

for a layer $k$ centered around $z_k$. The response from each layer is computed within DFPT. The layers are perturbed by a constant potential to probe the monopole response, then by a linear one (constant field) to probe the dipole response:

$$V_{\text{p,mono}}(q,z) = 1 \tag{A3}$$
$$V_{\text{p,dip}}(q,z) = z \tag{A4}$$

The density response $\delta n(q,z)$ is first extracted in reciprocal space $\delta n(q, G_z)$, with as many $G_z$ as the energy cutoff and supercell size dictates, then Fourier transformed back in real space, onto 1000 points $z \in [-c/2, c/2]$. Injecting the above perturbing potential into Eqs. (A1) with $\chi$ from (1), the density response to the monopole perturbation gives $Q(q)f(q, z - z_0)$ while the dipole one gives $P(q)g(q, z - z_0)$. Those quantities are computed on 10 $\mathbf{q}$-points in the range of values relevant for transport ($0 - 0.26$ Å$^{-1}$), and interpolated (scipy, quadratic spline) on finer sets of $q$-points. The $Q, P$ parameters are defined as the integrals over $z$ and $f, g$ as the normalized profiles. Fig. 9 shows those quantities in GaSe.

### 2. VdWh electrostatics

The potential induced by the heterostructure is the sum of the potentials induced by each layer $k$:

$$V_{\text{ind}}(q,z) = \sum_k v^k_{\text{ind}}(q,z) \tag{A5}$$

To compute the response of the system, the essential approximation is a kind of interlayer mean field approximation. In particular, we assume that each layer responds to an effective external potential that is the sum of the external potential and the potentials induced in each of the other layers:

$$\begin{aligned} v^k_{\text{ind}}(q,z) =& v_c(q) \int e^{-q|z-z'|} \int \chi(q,z',z'') \Big[ V_{\text{ext}}(z'') \\ &+ \sum_{m \neq k} v^m_{\text{ind}}(q,z'') \Big] dz'' dz' \end{aligned} \tag{A6}$$

We replace $\chi$ by its expression Eq. (1), and re-write the result as a systems of $2N$ equations with $2N$ unknowns, where $N$ is the number of layers in the heterostructure and the unknowns are the induced potentials averaged on each layer using either $f$ or $g$ as weight.

Injecting $\chi$ from Eq. (1) into Eq. (A6), we obtain:

$$v^k_{\text{ind}}(q,z) = v_c(q) \left( Q_k(q) F_k(q, z - z_k) \left[ \bar{v}^{ext}_k(q) + \bar{v}_k(q) \right] + P_k(q) G_k(q, z - z_k) \left[ \bar{w}^{ext}_k(q) + \bar{w}_k(q) \right] \right) \tag{A7}$$

with

$$F_k(q,z) = \int e^{-q|z-z'|} f_k(q,z') dz' \tag{A8}$$
$$G_k(q,z) = \int e^{-q|z-z'|} g_k(q,z') dz' \tag{A9}$$

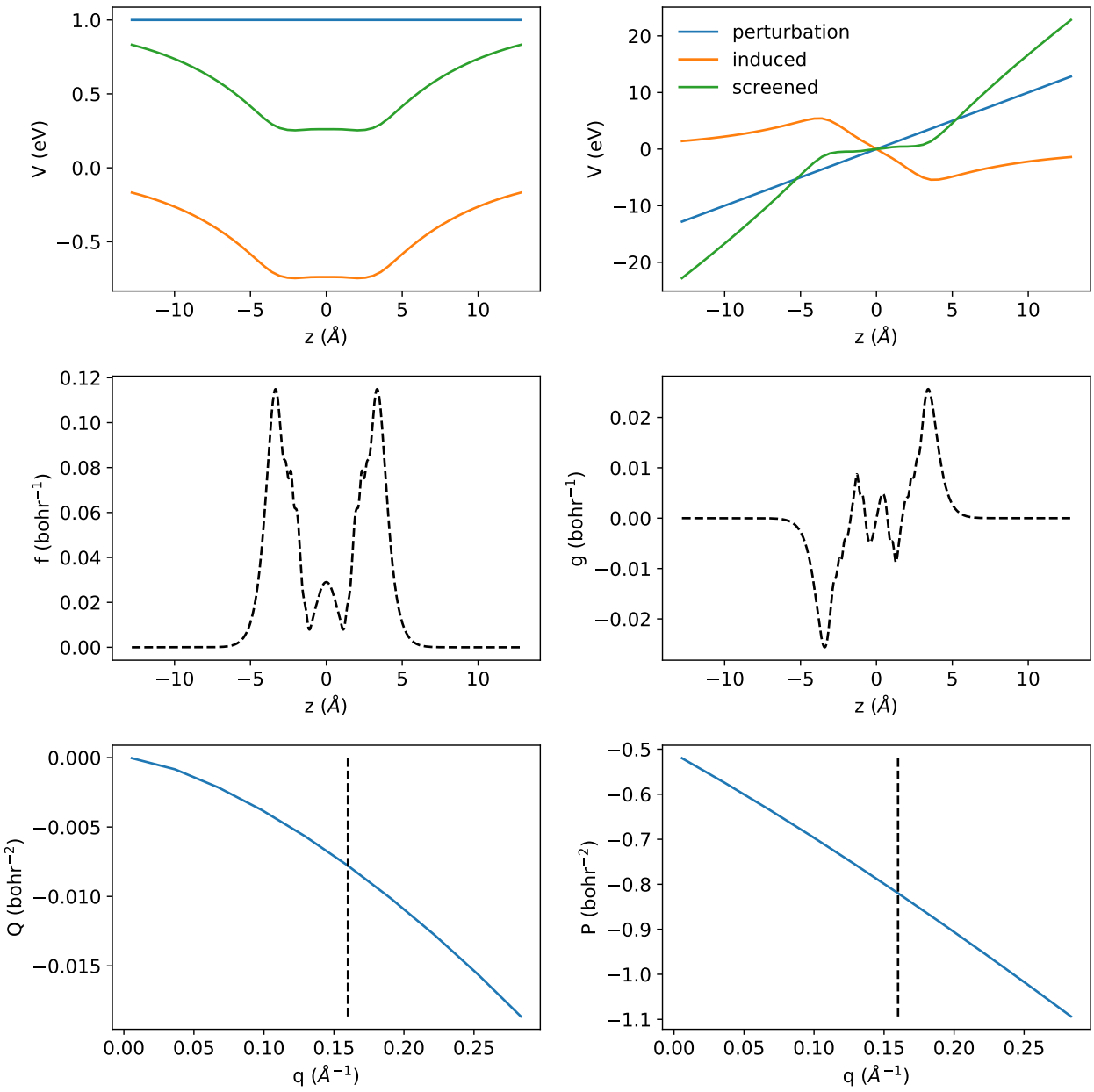


FIG. 9. The response of single-layer GaSe is extracted from DFPT. Left and right panels concern the monopole and dipole contributions to the response, respectively. The top panels show the bare perturbation (fixed at unity value), as well as the induced potential and the screened potential (sum of pertrubation and induced potential). The middle panels show the normalized out-of-plane profile functions $f$ and $g$. The bottom panels show the momentum-dependent amplitudes of the responses $Q$ and $P$. The dashed line corresponds to the momentum at which the potentials and profile functions are plotted.

$\bar{v}, \bar{w}$ designate projections/averages of the potentials over the monopole or dipole profiles:

$$\bar{v}_k^{ext}(q) = \int f_k(q,z')V_{\text{ext}}(z')dz' \tag{A10}$$

$$\bar{w}_k^{ext}(q) = \int g_k(q,z')V_{\text{ext}}(z')dz' \tag{A11}$$

$$\bar{v}_k(q) = \int f_k(q,z') \sum_{m\neq k} v_{\text{ind}}^m(q,z')dz' \tag{A12}$$

$$\bar{w}_k(q) = \int g_k(q,z') \sum_{m\neq k} v_{\text{ind}}^m(q,z')dz' \tag{A13}$$

Finally, multiplying both sides of Eq. (A7) by $f_p(q, z-z_p)$ or $g_p(q, z-z_p)$, integrating over $z$, and summing over $k \neq p$, one obtains a set of equations that $\bar{v}_p(q)$ and $\bar{w}_p(q)$ should satisfy at each $q$:

$$\bar{v}_p(q) = v_c(q) \sum_{k\neq p} \left( Q_k(q)C[f_p,f_k](q) \left[\bar{v}_k^{ext}(q) + \bar{v}_k(q)\right] + P_k(q)C[f_p,g_k](q) \left[\bar{w}_k^{ext}(q) + \bar{w}_k(q)\right]\right) \tag{A14}$$

$$\bar{w}_p(q) = v_c(q) \sum_{k\neq p} \left( Q_k(q)C[f_p,f_k](q) \left[\bar{v}_k^{ext}(q) + \bar{v}_k(q)\right] + P_k(q)C[g_p,g_k](q) \left[\bar{w}_k^{ext}(q) + \bar{w}_k(q)\right]\right) \tag{A15}$$

where $C[f_p, g_k](q)$ denotes the following double integral:

$$C[f_p,g_k](q) = \int\int f_p(q, z-z_p)e^{-q|z-z'|}g_k(q,z'-z_k)dz'dz \tag{A16}$$

$$\tag{A17}$$

and similarly for other combinations of $f, g$ functions with indices $p, k$.

Thus, we obtain a set of $2N$ equations with $2N$ unknowns, where $N$ is the number of layers. This is solved numerically at each momentum to find $v_k(q), w_k(q)$ for each layer $k$. The full $z$-dependency of the induced potentials are then recovered via Eq. (A7).

### 3. Fröhlich perturbation

Since the screening is computed within the VdWh via the electrostatics model, only the bare Fröhlich potential generated by polar-optical phonons is necessary here. In previous works[31], we assumed a generic square profile for the polarization density that is the source of the Fröhlich potential. Here we assume that the polarization follows the profile characterizing the materials' dielectric response found in DFPT $f$. The *bare* Fröhlich potential from layer $k$ centered around $z_k$ is then:

$$V_{\text{Fro,k}}(q,z) = C_Z^k \int e^{-q|z-(z'-z_k)|} f(z'-z_k)dz' \tag{A18}$$

For a layer centered around $z_k$. $C_Z^k$ is defined in each layer as:

$$C_Z^k = \frac{2\pi e^2}{A} \sum_a \frac{\mathbf{e_q} \cdot Z_a^k \cdot \mathbf{e}_{\Gamma,LO}^a}{\sqrt{2M_a\omega_{\Gamma,LO}}} \tag{A19}$$

where $A$ is the area of the unit cell, $a$ is an atomic index, $\mathbf{e_q} = \mathbf{q}/|\mathbf{q}|$, $Z_a^k$ are the Born effective charges of atom $a$ in layer $k$, $M_a$ is the mass of atom $a$, and $\omega_{\Gamma,LO}, \mathbf{e}_{\Gamma,LO}^a$ are the frequency and eigenvector of the LO mode at $\Gamma$.

Note that we include an extra electron charge factor $e$ in the definition of the potential. Strictly speaking, $V$ is the electric potential *energy* of a test charge $e$ within the potential. The variation of $C_Z$ as a function of $\mathbf{q}$ due to the phonon eigenvector and frequency are neglected : the values at $\Gamma$ are used. DFPT calculations in the GaSe and BN give $C_Z = 1.124$ and $1.994$ eV, respectively. The total Fröhlich potential is then a sum of the potentials from each "activated" layer, usually one material at a time, $V_{\text{Fro}}(q,z) = \sum_k V_{\text{Fro,k}}(q,z)$. To compute the corresponding electron-phonon coupling strength on layer $m$, the potential is then averaged over the profile of layer $m$: $g_{\text{Fro,m}}(q) = \int V_{\text{Fro}}(q,z)f_m(z-z_m)dz$ .

### 4. Free-carrier screening

The following is necessary to model free-carrier screening from the carrier density injected into the operating material, GaSe. The non-interacting density response function[14,19,50] is evaluated numerically using the band structure of the materials on a fine grid of $\mathbf{k}$-points

($96 \times 96$ for GaSe):

$$\chi_0(T=0,q) = -\frac{2FF(q)}{(2\pi)^2}\int d^2\mathbf{k}\frac{n_{FD}(\varepsilon_{\mathbf{k}}) - n_{FD}(\varepsilon_{\mathbf{k+q}})}{\varepsilon_{\mathbf{k+q}} - \varepsilon_{\mathbf{k}}} \tag{A20}$$

$$\chi_0(T,q) = \int \frac{\chi_0(q, T=0, \varepsilon_F = \varepsilon)}{4k_BT\cosh^2(\varepsilon_F(T) - \varepsilon/2k_BT)}d\varepsilon \tag{A21}$$

where $n_{FD}$ is the Fermi-Dirac occupation (which also depends on the chemical potential and the temperature) and the form factor FF(q) is computed using the monopole profile function $f$.

$$FF(q) = \int f(z-z_0)\int e^{-q|z-z'|}f(z'-z_0)dzdz' \tag{A22}$$

Note that this form factor relates the $Q(q)$ parameters to an (interacting) response function $\tilde{\chi}(q)$ that would be integrated in the out-plane-direction and would include only the monopole response $\tilde{\chi}(q) = Q(q)FF(q)$. The free-carrier response is combined with the dielectric response already in the model within RPA. In practice, the non-interacting response functions are added $\tilde{\chi}_0 = \tilde{\chi}_0^d + \tilde{\chi}_0^f$ ($d$ for dielectric, $f$ for free-carrier), the interacting response function is recomputed as $\tilde{\chi}(q) = \tilde{\chi}_0(q)/(1 - v_c(q)\tilde{\chi}_0(q))$ and a new $Q(q) = \tilde{\chi}(q)/FF(q)$ is injected in the solver.

### 5. Comparison with QEH model

The QEH model is similar to our approach but they differ on the following points: i) In QEH, the linear density response function is computed as in Ref. 51 then projected on two potential profile functions for monopole and dipole contributions. In our approach, the full density response to monopole and dipole perturbing potentials is directly interpolated on the **q**-points in which we are interested. By avoiding the projection on basis functions for the potentials, we keep the full $z$-dependency of the induced potentials during the process of solving the electrostatics. In QEH, a 1D Poisson equation in the out-of-plane direction needs to be solved at the end of the process to recover this $z$-dependency. ii) In QEH, the combination of the responses is achieved within the Dyson equation formalism. We employ a somewhat simpler electrostatic model. As far as we can tell, under the "interlayer mean-field" approximation, also used in QEH, both formalisms are equivalent. iii) QEH allows for a dynamical treatment of the responses, while our method is presently limited to the static limit. iv) QEH enables the treatment of anisotropic materials, while we stay in the isotropic case. v) Concerning free carrier screening, we arrived independently at a very similar approach (free carrier screening was added only very recently in the QEH method[19]). There are some pratical difference the calculations. QEH makes use of the quadratic band approximation to compute $\chi_0$, while it is evaluated numerically on the full band structure in our case. Also, we account for form factors effects. We don't expect a significant difference to arise from those differences.

Overall, the methods were developed with different quantities and applications in mind. Our approach is centered around potentials and their variations as a function of momentum $q$ and out-of-plane position $z$. The system can easily be perturbed by an arbitrary potential (Fröhlich in this work), and the response of each individual layer as well as the total effective potential can be easily extracted, bringing a clear picture of the underlying electrostatics. QEH focuses more macroscopically averaged quantities like the dielectric function and the underlying potentials are less accessible. We also have access to the dielectric function in our framework and we have checked that it agrees with the QEH one in multilayer BN.

[1] Chao Li, Peng Zhou, and David Wei Zhang, "Devices and applications of van der Waals heterostructures," Journal of Semiconductors **38**, 031005 (2017).

[2] Shi Jun Liang, Bin Cheng, Xinyi Cui, and Feng Miao, "Van der Waals Heterostructures for High-Performance Device Applications: Challenges and Opportunities," Advanced Materials **32**, 1903800 (2020).

[3] C R Dean, A F Young, I Meric, C Lee, L Wang, S Sorgenfrei, K Watanabe, T Taniguchi, P Kim, K L Shepard, and J Hone, "Boron nitride substrates for high-quality graphene electronics." Nature nanotechnology **5**, 722–6 (2010).

[4] F. Cadiz, E. Courtade, C. Robert, G. Wang, Y. Shen, H. Cai, T. Taniguchi, K. Watanabe, H. Carrere, D. Lagarde, M. Manca, T. Amand, P. Renucci, S. Tongay, X. Marie, and B. Urbaszek, "Excitonic Linewidth Approaching the Homogeneous Limit in MoS2-Based van der Waals Heterostructures," Physical Review X **7**, 021026 (2017), arXiv:1702.00323.

[5] André K Geim and I V Grigorieva, "Van der Waals heterostructures." Nature **499**, 419–425 (2013), arXiv:1307.6718.

[6] K. S. Novoselov, A. Mishchenko, A. Carvalho, and A. H. Castro Neto, "2D materials and van der Waals heterostructures," Science **353**, aac9439 (2016).

[7] Klaas Jan Tielrooij, Niels C.H. Hesp, Alessandro Principi, Mark B. Lundeberg, Eva A.A. Pogna, Luca Banszerus, Zoltán Mics, Mathieu Massicotte, Peter Schmidt, Diana Davydovskaya, David G. Purdie, Ilya Goykhman, Giancarlo Soavi, Antonio Lombardo, Kenji Watanabe, Takashi Taniguchi, Mischa Bonn, Dmitry Turchinovich, Christoph Stampfer, Andrea C. Ferrari, Giulio Cerullo, Marco Polini, and Frank H.L. Koppens, "Out-of-plane heat transfer in van der Waals stacks through electron-hyperbolic phonon coupling," Nature Nanotechnology **13**, 41–46 (2018), arXiv:1702.03766.

[8] Pasqual Rivera, Hongyi Yu, Kyle L Seyler, Nathan P Wilson, Wang Yao, and Xiaodong Xu, "Interlayer valley excitons in heterobilayers of transition metal dichalcogenides," Nature Nanotechnology **13**, 1004–1015 (2018).

[9] T. Wakamura, F. Reale, P. Palczynski, S. Guéron, C. Mattevi, and H. Bouchiat, "Strong Anisotropic Spin-Orbit Interaction Induced in Graphene by Monolayer WS2," Physical Review Letters **120**, 106802 (2018).

[10] M. Kim, S. G. Xu, A. I. Berdyugin, A. Principi, S. Slizovskiy, N. Xin, P. Kumaravadivel, W. Kuang, M. Hamer, R. Krishna Kumar, R. V. Gorbachev, K. Watanabe, T. Taniguchi, I. V. Grigorieva, V. I. Fal'ko, M. Polini, and A. K. Geim, "Control of electron-electron interaction in graphene by proximity screenings," Nature Communications **11**, 2339 (2020), arXiv:1911.10128.

[11] Meeghage Madusanka Perera, Ming Wei Lin, Hsun Jen Chuang, Bhim Prasad Chamlagain, Chongyu Wang, Xuebin Tan, Mark Ming Cheng Cheng, David Tománek, and Zhixian Zhou, "Improved carrier mobility in few-layer MoS2 field-effect transistors with ionic-liquid gating," ACS Nano **7**, 4449–4458 (2013).

[12] Felix Riederer, Thomas Grap, Sergej Fischer, Marcel R. Mueller, Daichi Yamaoka, Bin Sun, Charu Gupta, Klaus T. Kallis, and Joachim Knoch, "Alternatives for Doping in Nanoscale Field-Effect Transistors," Physica Status Solidi (A) Applications and Materials Science **215**, 1–16 (2018).

[13] Wei Zhao, Sheng Bi, Cheng Zhang, Philip D. Rack, and Guang Feng, "Adding Solvent into Ionic Liquid-Gated Transistor: The Anatomy of Enhanced Gating Performance," ACS Applied Materials and Interfaces **11**, 13822–13830 (2019).

[14] Nan Ma and Debdeep Jena, "Charge scattering and mobility in atomically thin semiconductors," Physical Review X **4**, 011043 (2014).

[15] Thibault Sohier, Marco Gibertini, and Nicola Marzari, "Profiling novel high-conductivity 2d semiconductors," 2D Materials (2020).

[16] Thibault Sohier, Matteo Calandra, and Francesco Mauri, "Density functional perturbation theory for gated two-dimensional heterostructures: Theoretical developments and application to flexural phonons in graphene," Physical Review B **96**, 075448 (2017), arXiv:1705.04973.

[17] Kirsten Andersen, Simone Latini, and Kristian S. Thygesen, "Dielectric Genome of van der Waals Heterostructures," Nano Letters **15**, 4616–4621 (2015), arXiv:1506.02463.

[18] Kristian Sommer Thygesen, "Calculating excitons, plasmons, and quasiparticles in 2D materials and van der Waals heterostructures," 2D Materials **4**, 022004 (2017).

[19] M. N. Gjerding, L. S. R. Cavalcante, Andrey Chaves, and K. S. Thygesen, "Efficient Ab Initio Modeling of Dielectric Screening in 2D van der Waals Materials: Including Phonons, Substrates, and Doping," The Journal of Physical Chemistry C **124**, 11609–11616 (2020).

[20] Zhizhan Qiu, Maxim Trushin, Hanyan Fang, Ivan Verzhbitskiy, Shiyuan Gao, Evan Laksono, Ming Yang, Pin Lyu, Jing Li, Jie Su, Mykola Telychko, Kenji Watanabe, Takashi Taniguchi, Jishan Wu, A. H. Castro Neto, Li Yang, Goki Eda, Shaffique Adam, and Jiong Lu, "Giant gate-tunable bandgap renormalization and excitonic effects in a 2D semiconductor," Science Advances **5**, eaaw2347 (2019).

[21] Thibault Sohier, Davide Campi, Nicola Marzari, and Marco Gibertini, "Mobility of 2D materials from first principles in an accurate and automated framework," Physical Review Materials **2**, 114010 (2018), arXiv:1808.10808.

[22] Thibault Sohier, Marco Gibertini, Davide Campi, Giovanni Pizzi, and Nicola Marzari, "Valley-Engineering Mobilities in Two-Dimensional Materials," Nano Letters **19**, 3723–3729 (2019).

[23] Oliviero Bistoni, Paolo Barone, Emmanuele Cappelluti, Lara Benfatto, and Francesco Mauri, "Giant effective charges and piezoelectricity in gapped graphene," 2D Materials **6**, 045015 (2019), arXiv:1903.09407.

[24] Samuel Poncé, Wenbin Li, Sven Reichardt, and Feliciano Giustino, "First-principles calculations of charge carrier mobility and conductivity in bulk semiconductors and two-dimensional materials," Reports on Progress in Physics **83**, 036501 (2020), arXiv:1908.01733.

[25] Jinlong Ma, Dongwei Xu, Run Hu, and Xiaobing Luo, "Examining two-dimensional Fröhlich model and enhancing the electron mobility of monolayer InSe by dielectric engineering," Journal of Applied Physics **128**, 035107 (2020).

[26] Nobuya Mori and Tsuneya Ando, "Electronoptical-phonon interaction in single and double heterostructures," Physical Review B **40**, 6175–6188 (1989).

[27] Sankar Das Sarma and Bruce A. Mason, "Optical phonon

interaction effects in layered semiconductor structures," Annals of Physics **163**, 78–119 (1985).
[28] Peter Vogl, "Microscopic theory of electron-phonon interaction in insulators or semiconductors," Physical Review B **13**, 694–704 (1976).
[29] Jelena Sjakste, Nathalie Vast, Matteo Calandra, and Francesco Mauri, "Wannier interpolation of the electron-phonon matrix elements in polar semiconductors: Polar-optical coupling in GaAs," Physical Review B - Condensed Matter and Materials Physics **92**, 054307 (2015), arXiv:1508.06172.
[30] Carla Verdi and Feliciano Giustino, "Fr{ö}hlich Electron-Phonon Vertex from First Principles," Physical Review Letters **115**, 176401 (2015).
[31] Thibault Sohier, Matteo Calandra, and Francesco Mauri, "Two-dimensional Fröhlich interaction in transition-metal dichalcogenide monolayers: Theoretical modeling and first-principles calculations," Physical Review B **94**, 085415 (2016).
[32] S. Poncé, Y. Gillet, J. Laflamme Janssen, A. Marini, M. Verstraete, and X. Gonze, "Temperature dependence of the electronic structure of semiconductors and insulators," Journal of Chemical Physics **143**, 102813 (2015), arXiv:1504.05992.
[33] .
[34] Leopold Talirz, Snehal Kumbhar, Elsa Passaro, Aliaksandr V. Yakutovich, Valeria Granata, Fernando Gargiulo, Marco Borelli, Martin Uhrin, Sebastiaan P. Huber, Spyros Zoupanos, Carl S. Adorf, Casper Welzel Andersen, Ole Schütt, Carlo A. Pignedoli, Daniele Passerone, Joost VandeVondele, Thomas C. Schulthess, Berend Smit, Giovanni Pizzi, and Nicola Marzari, "Materials Cloud, a platform for open computational science," Scientific Data **7**, 299 (2020), arXiv:2003.12510.
[35] Nicolas Mounet, Marco Gibertini, Philippe Schwaller, Davide Campi, Andrius Merkys, Antimo Marrazzo, Thibault Sohier, Ivano Eligio Castelli, Andrea Cepellotti, Giovanni Pizzi, Nicola Marzari, Davide Campi, Andrius Merkys, Antimo Marrazzo, Thibault Sohier, Ivano Eligio Castelli, Andrea Cepellotti, Giovanni Pizzi, and Nicola Marzari, "Two-dimensional materials from high-throughput computational exfoliation of experimentally known compounds," Nature Nanotechnology **13**, 246–252 (2018), arXiv:1611.05234.
[36] .
[37] Guillaume Brunin, Henrique Pereira Coutada Miranda, Matteo Giantomassi, Miquel Royo, Massimiliano Stengel, Matthieu J. Verstraete, Xavier Gonze, Gian-Marco Rignanese, and Geoffroy Hautier, "Electron-Phonon beyond Fröhlich: Dynamical Quadrupoles in Polar and Covalent Solids," Physical Review Letters **125**, 136601 (2020), arXiv:2002.00628.
[38] Guillaume Brunin, Henrique Pereira Coutada Miranda, Matteo Giantomassi, Miquel Royo, Massimiliano Stengel, Matthieu J. Verstraete, Xavier Gonze, Gian-Marco Rignanese, and Geoffroy Hautier, "Phonon-limited electron mobility in Si, GaAs, and GaP with exact treatment of dynamical quadrupoles," Physical Review B **102**, 94308 (2020), arXiv:2002.00630.
[39] Vatsal A. Jhalani, Jin-Jian Zhou, Jinsoo Park, Cyrus E. Dreyer, and Marco Bernardi, " Piezoelectric Electron-Phonon Interaction from Ab Initio Dynamical Quadrupoles: Impact on Charge Transport in Wurtzite GaN ," Physical Review Letters **125**, 136602 (2020), arXiv:2002.08351.
[40] Jinsoo Park, Jin-Jian Zhou, Vatsal A. Jhalani, Cyrus E. Dreyer, and Marco Bernardi, "Long-range quadrupole electron-phonon interaction from first principles," Physical Review B **102**, 125203 (2020), arXiv:2003.13782.
[41] Thibault Sohier, Marco Gibertini, Matteo Calandra, Francesco Mauri, and Nicola Marzari, "Breakdown of Optical Phonons' Splitting in Two-Dimensional Materials," Nano Letters **17**, 3758–3763 (2017), arXiv:1612.07191.
[42] Thibault Sohier, Matteo Calandra, and Francesco Mauri, "Density-functional calculation of static screening in two-dimensional materials: The long-wavelength dielectric function of graphene," Physical Review B **91**, 165428 (2015), arXiv:1503.02530v1.
[43] Paolo Giannozzi, Stefano Baroni, Nicola Bonini, Matteo Calandra, Roberto Car, Carlo Cavazzoni, Davide Ceresoli, Guido L Chiarotti, Matteo Cococcioni, Ismaila Dabo, Andrea Dal Corso, Stefano de Gironcoli, Stefano Fabris, Guido Fratesi, Ralph Gebauer, Uwe Gerstmann, Christos Gougoussis, Anton Kokalj, Michele Lazzeri, Layla Martin-Samos, Nicola Marzari, Francesco Mauri, Riccardo Mazzarello, Stefano Paolini, Alfredo Pasquarello, Lorenzo Paulatto, Carlo Sbraccia, Sandro Scandolo, Gabriele Sclauzero, Ari P Seitsonen, Alexander Smogunov, Paolo Umari, Renata M Wentzcovitch, Andrea Dal Corso, Guido Fratesi, Stefano De Gironcoli, Ralph Gebauer, Uwe Gerstmann, Christos Gougoussis, Anton Kokalj, Layla Martin-Samos, Nicola Marzari, Francesco Mauri, Riccardo Mazzarello, Stefano Paolini, Alfredo Pasquarello, Lorenzo Paulatto, Carlo Sbraccia, Sandro Scandolo, Ari P Seitsonen, Alexander Smogunov, Paolo Umari, and Renata M Wentzcovitch, "QUANTUM ESPRESSO: a modular and open-source software project for quantum simulations of materials." Journal of Physics: Condensed Matter **21**, 395502 (2009), arXiv:0906.2569.
[44] P Giannozzi, O Andreussi, T Brumme, O Bunau, M Buongiorno Nardelli, M Calandra, R Car, C Cavazzoni, D Ceresoli, M Cococcioni, N Colonna, I Carnimeo, A Dal Corso, S. De Gironcoli, P Delugas, R. A. Distasio, A Ferretti, A Floris, G Fratesi, G Fugallo, R Gebauer, U Gerstmann, F Giustino, T Gorni, J Jia, M Kawamura, H. Y. Ko, A Kokalj, E. Kücükbenli, M Lazzeri, M Marsili, N Marzari, F Mauri, N. L. Nguyen, H. V. Nguyen, A. Otero-De-La-Roza, L Paulatto, S Poncé, D Rocca, R Sabatini, B Santra, M Schlipf, A P Seitsonen, A Smogunov, I Timrov, T Thonhauser, P Umari, N Vast, X Wu, and S Baroni, "Advanced capabilities for materials modelling with Quantum ESPRESSO," Journal of Physics Condensed Matter **29**, 465901 (2017), arXiv:1709.10010.
[45] Gianluca Prandini, Antimo Marrazzo, Ivano E. Castelli, Nicolas Mounet, and Nicola Marzari, "Precision and efficiency in solid-state pseudopotential calculations," npj Computational Materials **4**, 72 (2018), arXiv:1806.05609.
[46] D. R. Hamann, "Optimized norm-conserving Vanderbilt pseudopotentials," Physical Review B **88**, 085117 (2013).
[47] M. J. van Setten, M. Giantomassi, E. Bousquet, M. J. Verstraete, D. R. Hamann, X. Gonze, and G. M. Rignanese, "The PSEUDODOJO: Training and grading a 85 element optimized norm-conserving pseudopotential table," Computer Physics Communications **226**, 39–54 (2018), arXiv:1710.10138.
[48] Giovanni Pizzi, Andrea Cepellotti, Riccardo Sabatini, Nicola Marzari, and Boris Kozinsky, "AiiDA: automated interactive infrastructure and database for computational

science," Computational Materials Science **111**, 218–230 (2016).

[49] Sebastiaan. P. Huber, Spyros Zoupanos, Martin Uhrin, Leopold Talirz, Leonid Kahle, Rico Häuselmann, Dominik Gresch, Tiziano Müller, Aliaksandr V. Yakutovich, Casper W. Andersen, Francisco F. Ramirez, Carl S. Adorf, Fernando Gargiulo, Snehal Kumbhar, Elsa Passaro, Conrad Johnston, Andrius Merkys, Andrea Cepellotti, Nicolas Mounet, Nicola Marzari, Boris Kozinsky, and Giovanni Pizzi, "AiiDA 1.0, a scalable computational infrastructure for automated reproducible workflows and data provenance," Scientific Data **7**, 300 (2020), arXiv:2003.12476.

[50] Pierre F. Maldague, "Many-body corrections to the polarizability of the two-dimensional electron gas," Surface Science **73**, 296–302 (1978).

[51] Jun Yan, Jens. J. Mortensen, Karsten W. Jacobsen, and Kristian S. Thygesen, "Linear density response function in the projector augmented wave method: Applications to solids, surfaces, and interfaces," Physical Review B **83**, 245122 (2011).